Precompound decay calculations for reactions induced by 10—100 MeV/nucleon heavy ions

M. Blann
Lawrence Livermore National Laboratory, University of California, Livermore, California 94550
(Received 12 November 1984)

The Boltzmann master equation model has been applied to the question of precompound nucleon deexcitation of reactions induced by 10—100 MeV/nucleon (c.m.) heavy ions. Test systems of $^{16}O+^{60}Ni$ and $^{27}Al+^{86}Kr$ were selected. Experimental neutron spectra in coincidence with evaporation residue and fission fragments from the $^{20}Ne+^{165}Ho$ system (due to Holub *et al.*) were reproduced quite well by the master equation with exciton numbers between 20 and 23. Exciton values of projectile mass and projectile mass plus 3 were therefore used in the extrapolations of the master equation. Results show major fractions of the excitation and up to 35 nucleons removed during the coalescence-equilibration period. The linear momentum transfer predicted by the master equation is shown to be in good agreement with a broad range of data. Calculations are provided as to the range of angular momenta which may be carried off by the precompound cascade.

I. INTRODUCTION

A very large experimental effort is being expended in the investigation of reactions induced by heavy ions of energies in excess of 10 MeV/nucleon. An important consideration in this energy range is the prompt nucleonic cascade which can greatly alter the excitation energy available for other processes, e.g., fissionlike, or phenomena due to a somewhat relaxed composite system. In order to interpret many of the observable reaction properties it is helpful to have a model which is useful in predicting this precompound nucleonic cascade background.

In the present work we will explore the application of the Boltzmann master equation using the code of Harp, Miller, and Berne,[1,2] as modified by Blann and Harp to consider heavy ion reactions.[3,4] We will predict precompound nucleon decay properties of the projectile-target pairs $^{16}O+^{60}Ni$ and $^{27}Al+^{86}K$, at projectile energies of 10—100 MeV/nucleon (c.m.). In Sec. II we will review the master equation model, and in particular the key question of the parameters which may influence the initial exciton energy distribution as the target-projectile pair makes contact and coalesces. In Sec. III we will present results of the calculations for the two sample systems selected. We will include estimates of the linear momentum transfer, which will be compared with experimental results for various projectile-target pairs. In Sec. IV we will summarize our results, and discuss the types of experimental measurements which would test the model under consideration more rigorously as to its ability to reproduce the main aspects of the physics involved, and which might also permit improvements in the important exciton distribution assumption which contains much of the detailed mechanistic information of the model.

II. MASTER EQUATION MODEL

A. Boltzmann master equation

The code which we use was written by Harp *et al.*[1,2] to consider the relaxation to equilibrium of high energy nucleon induced reactions. It was later used by Harp and Miller[2] for investigating precompound decay for nucleon-induced reactions in the region of a few tens of MeV of excitation. This code was modified by Harp and Blann for use in heavy ion reaction studies.[3,4]

The code used considers a two-component (neutron and proton) fermion gas. An energy space is considered which is initially filled below the Fermi energy. Excitation energy is introduced into the system by bringing nucleons into the potential well in positions above the Fermi energy. The relaxation of these particles by either internal nucleon-nucleon (N-N) scattering, or by emission into the continuum, is followed versus time using coupled differential equations deriving their rates from phase space considerations.

The set of coupled differential equations used, as stated, was for a two-component fermion gas. However, it is more easily summarized in terms of a one-component fermion gas,

$$\frac{d(n_i g_i)}{dt} = \sum_{j,k,l} \omega_{kl,ij} g_k n_k g_l n_l (1-n_j)(1-n_i) g_i g_j - \sum_{j,k,l} \omega_{ij,kl} g_i n_i g_j n_j (1-n_k)(1-n_l) g_k g_l - n_i g_i \omega_{i,i'} g_{i'} + \frac{d}{dt}(n_i g_i)\text{fus} , \quad (1)$$

where n_i is the average occupation number and g_i the number of single particle states per MeV in an energy interval 1 MeV wide measured from the bottom of the compound nucleus well. The $\omega_{ab,cd}$ are the transition probabilities for nucleons in initial states a and b to scatter into final states c and d; they are evaluated from free nucleon-nucleon scattering cross sections. The fractional occupation numbers $(1-n_i)$ which multiply the free

nucleon-nucleon collision rates give the Pauli exclusion correction. The $\omega_{i,i'}$ give the rate for a particle at energy i within the nucleus to go to energy i' outside the nucleus. The first two terms of Eq. (1) give the rates of scattering particles into and out of the interval i by two-body (N-N) collisions, while the third term gives the rate of emission into the continuum. If this emission takes place before an internal equilibrium nucleon distribution is attained, the contribution is part of the precompound spectrum. (An equilibrium distribution is characterized by an equal *a priori* population of every possible particle-hole configuration.) For details of quantitative input to the relevant transition rates we refer to earlier works.[1,2]

The fourth term in Eq. (1) contains a major portion of the physics in applying the master equation to heavy ion reactions. It represents the time dependent injection of excitons into the coalescing system. This should involve the microscopic aspects of the energy dissipation mechanism, and makes the model useful in testing energy dissipation models. In this work, as in earlier work, we will make simple phase space arguments similar to those used in exciton models over the past decade.[4–6] We discuss the evaluation of the "injection" term of Eq. (1) in the next subsection.

B. Exciton injection distributions

The basis of our approach is the assumption that, for the interacting nuclei, the center of mass and Fermi momenta of the participant nucleons may couple in an equal *a priori*, energy conserving fashion.[6] This is an extension of the argument used in precompound decay models in which, e.g., an α projectile is characterized by a four-exciton distribution. But we must consider the ways in which a heavy ion reaction differs from a light projectile induced reaction, so that we may judge success in our heavy ion reaction test with consideration of our uncertainty limits. We therefore next engage in a speculative discussion of this point.

In a nucleon induced reaction, we may clearly view the process as one exciton (the projectile) entering the nuclear potential. It may either be emitted, or it may scatter internally. This is clearly a one-exciton initial configuration which may go to the three, five, etc., exciton configurations via two-body interactions. Consider next a collision between symmetric heavy ions (e.g., Kr + Kr). Here as the nuclei come into contact, neither nucleus is clearly the target and the other the projectile. Nucleons will be expected to pass back and forth between both partners.[7] We might therefore expect a larger number of degrees of freedom (exciton number) to characterize this reaction relative to the "projectile" nucleon number than for a nucleon or α induced reaction. In addition collective degrees of freedom may be important in the heavy ion reaction.

For nucleon induced reactions it is clear that the exciton phase space properly includes the capture Q value. For heavy ion reactions the dinuclear shape is very deformed during the early stages of interaction during which nucleonic relaxation is expected to begin taking place.[8] This shape is far from the compound nucleus equilibrium shape, and therefore a significant amount of excitation may be unavailable for nucleonic (exciton) excitation. Additionally, large amounts of rotational energy may be unavailable to nucleon excitation in heavy ion reactions.[9] These collective effects are expected to be dependent on the particular target-projectile combination, impact parameter, and bombarding energy.

It is clear that the exciton distribution for heavy ion reactions is not expected to be as straightforward as for light ion induced reactions. The real challenge may be in the formulation of reaction models for the dissipation process to give time dependent exciton spectra which may be used in Eq. (1) to generate nucleon emission spectra, which in turn may be compared with experimental results. The dynamics of the coalescence process may be important in determining the exciton spectra; however, in this work we will simply use distributions characterized by exciton numbers which seem to give a reasonable reproduction of some experimental results, in order to generate extrapolated results. We will use single exciton numbers to represent the initial energy partitions, recognizing that careful considerations of the problem would lead at least to distributions represented by weighted sums over a range of exciton numbers, with some additional energy constraint for collective effects. We do this because our goal is use of the master equation to provide first-order guidance of the expected nucleon cascade, rather than to solve the problem of microscopic injection. We feel that more extensive experimental results are necessary to guide the microscopic modeling.

The absolute maximum energy a single exciton could have as two heavy ions begin to coalesce would be the excitation energy of the compound nucleus, if it were formed; of course we would expect a vanishingly small probability of such a rare coupling. Energy tied up in collective modes (rotation, deformation) would be expected to decrease the hypothetical maximum exciton energy below the compound nucleus value. The exciton state density expression[10] apportions a maximum excitation energy E among p particles and h holes with equal *a priori* probability of energy per exciton (where $n = p + h$ is the exciton number),

$$N(E) = (E)^{n-1}/p!h!(n-1)! , \tag{2}$$

where the energy E is expressed in units of the excitation energy E^*, $E = gE^*$, and g is the single particle state density in levels/MeV. We will assume a hole number of zero for estimating initial exciton populations for heavy ion reactions.

We may integrate Eq. (2) over energy intervals of width ΔU to calculate the number of excitons in an energy interval between U and $U + \Delta U$,

$$N(U)\Delta U = [(E-U)^{n-1} - (E-U-\Delta U)^{n-1}]/E^{n-1} . \tag{3}$$

Equation (3) was used in earlier works[4] for treating heavy ion reactions, where it was assumed that some number of projectile excitons $n(t)$ entered the exciton mix at time t; $n(t)$ multiplied by Eq. (3) gives the energy distribution of these excitons, and this became the injection term of Eq.

(1). The number $n(t)$ for neutrons (protons) was calculated as the projectile neutron (proton) number times the fractional volume of the projectile which would pass through a plane in a single time increment (which in our calculations is 2×10^{-23} sec) at a constant velocity determined by the center of mass velocity at the top of the Coulomb barrier. We would expect realistic coalescence dynamics to cause large excursions from this value (mainly to longer mix times); however, increasing the coalescence period does not significantly affect the results of calculations with Eq. (1).

Use of Eq. (3) involves the implicit assumption that a single exciton may (with very minimal expectation) have the full energy available. This is quite reasonable for a nucleon induced reaction for which the incident nucleon begins with the full energy. However, for heavy ion reactions each nucleon has but a small fraction of the total energy. We argue that coupling with the Fermi motion makes a large portion of this energy available.[6] Consider as an example a reaction induced on a very heavy target by 10 MeV/nucleon ^{20}Ne. The total available excitation energy would be $\approx$200 MeV (if there were no collective restrictions). Yet if the Fermi energy were a maximum of 40 MeV, the maximum nucleon energy would be expected to be nearer $(\sqrt{10}+\sqrt{40})^2=90$ MeV. If nucleons in the half-density nuclear region were primarily responsible for the precompound processes, a lower effective Fermi energy and lower maximum exciton energy might be appropriate. The density region over which nucleon exchange is taking place is a significant consideration for the ultimate use of model calculations of the type presented herein.

These considerations would suggest that Eq. (3) be replaced by a distribution function giving the number of excitons in a given energy range when there is an equal *a priori* distribution of energy, but with the constraint that no exciton may have more than some energy F. If $C(E,n,F)$ is defined as the number of ways of distributing E identical objects (energy quanta) among n cells (excitons) such that no cell has more than F objects,

$$P(U)=\frac{C(E-U,n-1,F)}{C(E,n,F)} . \tag{4}$$

The value of $C(E,n,F)$ is given by

$$C(E,n,F)=\frac{1}{E!}\frac{d^E}{dx^E}(1+x+x^2\cdots x^F)^n . \tag{5}$$

We have used a subroutine[11] based on Eqs. (4) and (5) to provide the injection term of Eq. (1) in order to investigate the consequences of Fermi coupling constants on the exciton distribution function. We find that this constraint versus Eq. (3) is not important, and have used Eq. (3) in this work except where otherwise noted.

C. Exciton injection parameters

Before performing fairly global predictive calculations with the master equation model, we must consider how well experimental data are reproduced by this approach. Ideally we would like to test the model versus neutron and proton spectra in coincidence with evaporation residues, for incident heavy ions of energies in excess of 10 MeV/nucleon and over the entire energy range of interest. Some data are available for the reaction of ^{20}Ne + ^{165}Ho. In particular precompound neutron spectra in coincidence with fission fragments and evaporation residues were reported for 220, 290, and 402 MeV incident ^{20}Ne energy.[12]

In Fig. 1 we compare experimentally deduced spectra with results of the master equation calculation of Eq. (1) using Eqs. (4) and (5) for the exciton injection spectra, assuming that either 20 or 23 excitons partition the available excitation. The upper limits of excitation energy were used, i.e., the compound nucleus values which were 164, 228, and 326 MeV for incident ^{20}Ne energies of 220, 292, and 402 MeV, respectively. The experimental, angle integrated results shown in Fig. 1 are based on a Maxwellian fit to the high energy neutron spectra; the evaporationlike component (which is partially included in our calculated result) is not included in the experimental spectra of Fig. 1. The calculated results of Fig. 1 are absolute and unnormalized. The phase space arguments previously stated, coupled with the unadjusted nucleon-nucleon scattering cross sections which give the "spreading" rate, yield the results of Fig. 1. The degree of agreement between calculated and experimental spectra is somewhat subjective. We feel that the 20 exciton result is satisfacto-

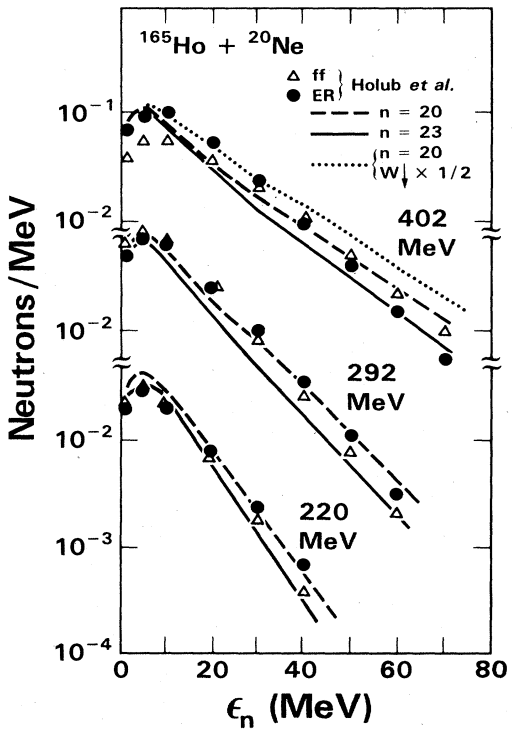

FIG. 1. Experimental and calculated precompound spectra for reactions induced by 220, 292, and 402 MeV (lab) ^{20}Ne ions on ^{165}Ho. The experimental points from Ref. 12 represent neutron spectra in coincidence with evaporation residues (open triangles) and fission fragments (closed circles). Calculated results are for initial exciton numbers of 20 (dashed curves) and 23 (line). A calculation using 20 excitons with the intranuclear transition rate divided by two is shown as a dotted curve for the 402 MeV case. All results are compared on an absolute, unnormalized basis.

ry for all three bombarding energies. The experimental results certainly seem "bracketed" by the 20 and 23 exciton results. [The trend of differences between experimental evaporation residue (ER) and fission coincident neutron spectra are suggestive of increased rotational energy with increased beam velocity for the fission-gated spectra.] Based on these observations we will use $n_0 = A_p$ and $A_p + 3$ for the calculations to be performed on the $^{16}O + {}^{60}Ni$ and $^{27}Al + {}^{86}Kr$ systems, giving a range of results, and indicating the sensitivity of results to the exciton number parameter.

For the case of 402 MeV incident ^{20}Ne energy we have performed a calculation ($n_0 = 20$) in which the intranuclear transition rate was half the default value. This would approximate the result expected if the nucleon exchange took place predominantly in nuclear matter of considerably less than half-density. This result (Fig. 1) may be seen to overestimate the experimental yields. Higher n_0 values would be required to get better agreement at the higher neutron energies with the reduced intranuclear transition rate. This may be the reason that Holub *et al.* found higher "best" exciton numbers than we find in this work, in their otherwise similar analysis of their spectra.[12]

Figure 1 indicates that the master equation gives a quite reasonable prediction of the high energy precompound nucleon spectra over a reasonably broad range of excitation. We will therefore use this approach to estimate some characteristics of the precompound cascade in heavy ion reactions both within this excitation range and beyond it. While it would be beneficial to have spectra similar to those of Fig. 1 to assess the validity of the calculation at higher energies, we are not aware of the availability of such data. We therefore proceed, leaving open the question of microscopic modeling of dynamic collective effects and their influence on the exciton distributions.

III. RESULTS AND DISCUSSION

In the previous section it was shown that the master equation calculation gives a quite satisfactory reproduction of the precompound neutron spectra for the systems analyzed (Fig. 1), with the parameter for the initial exciton selected to be equal to or several units greater than the projectile mass number. We now proceed to use the master equation as a tool to give a gross guide to the question of energy and nucleon loss during the coalescence-equilibration process, using an exciton number parameter based on the analysis of the preceding section.

We will consider two systems differing somewhat in mass and charge, $^{16}O + {}^{60}Ni$ and $^{27}Al + {}^{86}Kr$. A range of energies from 10 to 100 MeV/nucleon (c.m.) will be considered in order to show how the relaxation process changes with the available excitation energy. We will assume effective exciton numbers of 16 and of 19 for the ^{16}O induced reactions, and of 27 and of 30 for the ^{27}Al induced reactions. In Sec. III A we present a broad, general discussion of the deexcitation process; in Sec. III B, we consider the implications of the predicted nucleonic cascade on the average linear momentum transfer to the excited equilibrated reaction residues.

A. Precompound deexcitation

The decay characteristics predicted by the master equation are displayed graphically in Fig. 2 for the Al + Kr system for the assumption of 27 initial excitons; results for both test systems are summarized in Tables I and II for $n = A_p + 3$, and in Tables III and IV for $n = A_p$. The graphs in Fig. 2 show many of the predicted decay properties versus time for the example shown; characteristics of proton emission are similar to neutron emission. Similarly the $^{16}O + {}^{60}Ni$ system has the same features as the Al + Kr system. For these reasons we exhibit only one figure of this type. Discussion of Fig. 2(h) linear momentum transfer and of additional assumptions necessary to its calculation, is deferred to Sec. III B. Results similar to those shown in Fig. 2 for proton emission are available from the calculation and are summarized in Tables I–IV.

The time at which the infusion of nucleons from the projectile to the composite system is complete is indicated in Fig. 2(b) and in Tables I–IV. Determining the approximate time at which a given system has equilibrated is more subjective. We have taken the results in Fig. 2(b) and extrapolated the linear regions of the curves at long times to shorter times. The region first showing an acceleration in the rate of neutron emission is taken as the equilibration time. Dashed curves have been added in Fig. 2(b) to illustrate this procedure. The times for fusion and for equilibration are summarized in Tables I–IV. Both start from time zero defined as the time of the initial target-projectile contact, i.e., the beginning of the coalescence process.

In Tables I–IV we have multiplied the neutron (proton) multiplicities for precompound nucleons by the neutron (proton) binding energies. With the implicit assumption that the values used in the calculations represent reasonable averages, this allows us to estimate the total (kinetic plus binding) energy removed during equilibration. These results are summarized graphically in Fig. 3. One interesting trend in Fig. 3 is the decrease in rate of precompound excitation removal above 50 MeV/nucleon. For the case $n_0 = A_p$, the fractional results shown in Fig. 3 are not distinguishable for the two systems under consideration.

The figures and tables show a rapid increase of precompound decay as projectile energies exceed 10 MeV/nucleon, as pointed out earlier.[3,4,6] The systems may be seen to relax rapidly toward equilibrium following the conclusion of coalescence, i.e., in periods of the order of $2-5\times10^{-22}$ sec. Nonetheless these periods are in the range of the collective times required to go from contact to an equilibrium composite configuration (particularly in the "extra" push region), and from the compound shape to saddle. Many nucleons may be emitted during this time, considerably altering both the excitation energy and angular momentum of the hot, equilibrated residue. For example, for Al + Kr at 100 MeV/nucleon, our model calculation predicts approximately 35 nucleons (and probably additional d, t, α, etc., clusters) removed during this short period, and 1800 of the 2700 MeV of maximum available excitation removed. Interpretation of, e.g., coincident fission fragments in such an experiment would

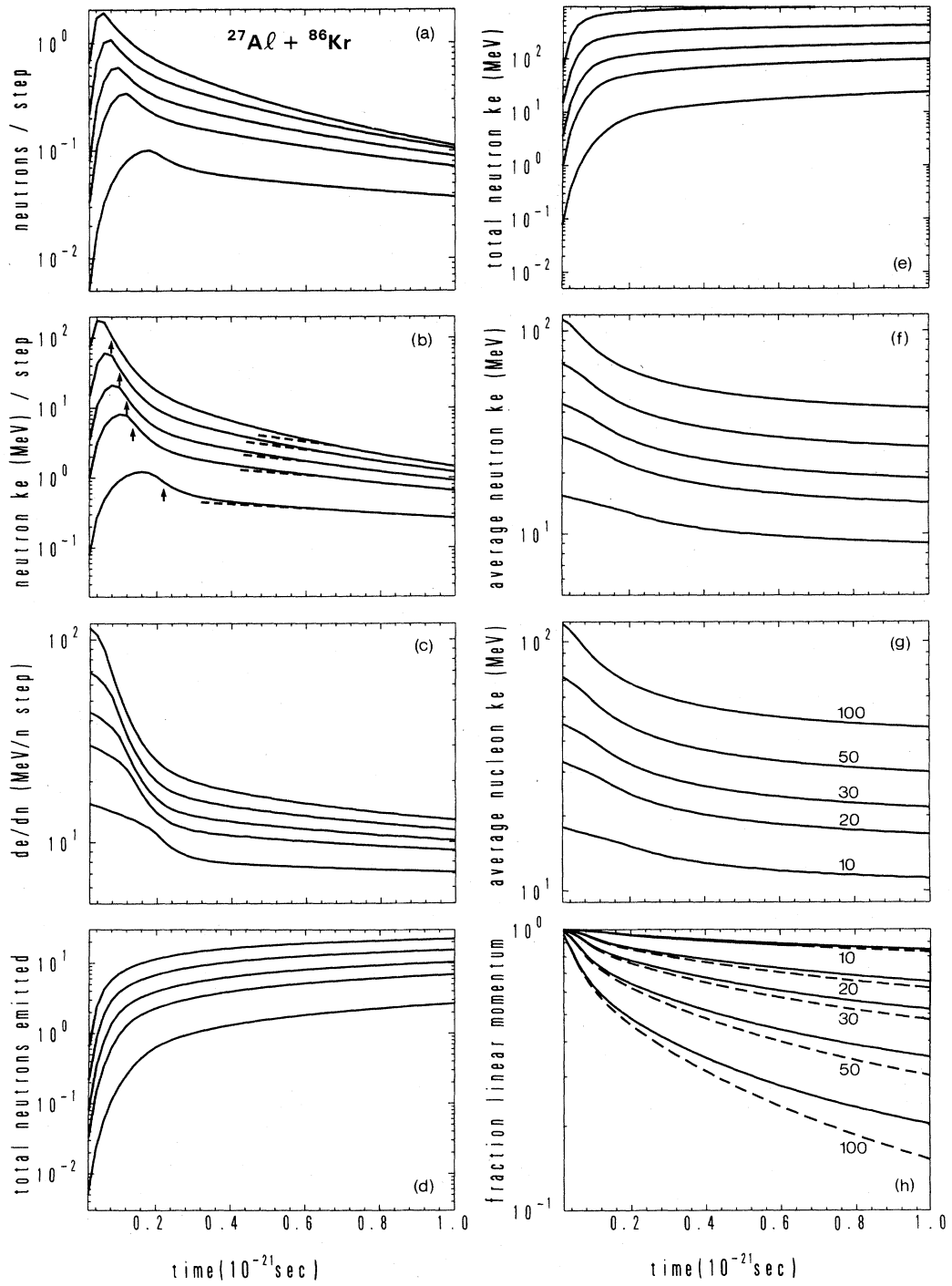

FIG. 2. Calculated precompound decay quantities versus time for reactions induced by 10, 20, 30, 50, and 100 MeV/nucleon (c.m.) ^{27}Al ions on ^{86}Kr. For each bombarding energy the figure shows the following versus time: (a) the number of neutrons emitted during each time step (Δt) (2×10^{-23} sec) of the computation; (b) the kinetic energy removed by neutrons during each Δt; (c) the energy per neutron removed during each Δt [i.e., the quotient of (b) by (a)]; (d) the total neutrons emitted up to time t; (e) the total kinetic energy removed by neutrons up to time t; (f) the average neutron energy of all neutrons emitted up to time t; (g) the average nucleon (neutron plus proton) kinetic energy removed up to time t; and (h) the fraction linear momentum remaining on the heavy residues up to time t. In (b) the up arrows indicate the time at which fusion was complete for each incident energy; the intersections of the dashed lines with the calculated curves were used to estimate an equilibration time. The incident energies are shown in (g) and (h). The ordering shown in (g) is valid for (a)—(g). In (h) the dashed curves represent the calculated linear momentum if it is assumed that all nucleons are emitted at 0° to the beam, i.e., if the angular correction of Eq. (6) is not made.

TABLE I. Calculated decay prior to equilibration for reactions of $^{27}Al + {}^{86}Kr$ assuming a 30 exciton partition.

E_{lab} ^{27}Al (MeV)	$t_{eq} \times 10^{22}$ (sec)	$t_{fus} \times 10^{22}$ (sec)	$\frac{p_{11}}{p_{beam}}$ [a]	Δl [b] ($\hbar$)	N_n [c]	N_p [d]	KE_n [e] (MeV)	KE_p [f] (MeV)	ΔE [g] (MeV)	$\Delta E/E$ [h]	v_{rel} [i]	$(E/A)_{c.m.}$ (MeV/nucleon)
355	4.7	2.2	0.92	13	1.28	0.65	12.2	10.4	40	0.15	3.1	10
710	4.8	1.4	0.79	48	3.95	2.42	62	54	170	0.32	4.8	20
1065	5.1	1.2	0.67	92	6.74	4.41	137	121	350	0.44	6.0	30
1775	6.6	1.0	0.48	187	12.2	8.47	334	295	800	0.60	7.9	50
3350	7.8	0.8	0.28	355	20.0	14.5	826	720	1830	0.68	10.8	100

[a]Estimated fraction of linear momentum transfer.
[b]Angular momentum removal prior to t_{eq}.
[c]Number of neutrons emitted prior to t_{eq}.
[d]Number of protons emitted prior to t_{eq}.
[e]Neutron kinetic energy removed prior to t_{eq}.
[f]Proton kinetic energy removed prior to t_{eq}.
[g]Sum of neutron plus proton kinetic and binding energy removed prior to t_{eq}.
[h]Ratio of energy removed by precompound particle emission to total available compound nucleus excitation energy.
[i]$\sqrt{(E_{lab} - V)/A_p}$ where V is the Coulomb barrier and A_p the projectile mass number (27).

TABLE II. Calculated decay prior to equilibration for reactions of $^{16}O + {}^{60}Ni$ assuming a 19 exciton partition (column headings are as defined in Table I).

E_{lab} ^{16}O (MeV)	$t_{eq} \times 10^{22}$ (sec)	$t_{fus} \times 10^{22}$ (sec)	$\frac{p_{11}}{p_{beam}}$	Δl ($\hbar$)	N_n	N_p	KE_n (MeV)	KE_p (MeV)	ΔE (MeV)	$\Delta E/E$	v_{rel}	$(E/A)_{c.m.}$ (MeV/nucleon)
141	3.8	2.2	0.98	1	0.16	0.20	1.15	2.4	6.6	0.06	2.4	7.0
218	3.8	1.8	0.94	5	0.52	0.56	5.2	8.3	23	0.13	3.2	10.8
314	4.2	1.4	0.88	12	1.05	1.15	13.7	20.4	54	0.22	4.1	15.5
800	5.0	0.8	0.64	59	4.05	1.15	99	119	291	0.46	6.9	39.5
1013	6.0	0.8	0.54	85	5.5	5.6	153	179	431	0.54	7.8	50.0
1600	6.1	0.6	0.41	137	8.0	8.0	305	332	780	0.62	9.8	79.0
2027	6.2	0.6	0.36	167	9.2	9.1	408	435	1007	0.63	11.1	100.0

TABLE III. Calculated decay prior to equilibration for reactions of $^{27}Al + {}^{86}Kr$ for $n=27$ (column headings are as defined in Table I).

E_{lab} ^{27}Al (MeV)	$t_{eq} \times 10^{22}$ (sec)	$t_{fus} \times 10^{22}$ (sec)	$\frac{p_{11}}{p_{beam}}$	Δl ($\hbar$)	N_n	N_p	KE_n (MeV)	KE_p (MeV)	ΔE (MeV)	$\Delta E/E$	v_{rel}	$(E/A)_{c.m.}$ (MeV/nucleon)
355	4.8	2.2	0.91	15	1.54	0.81	15.7	13.5	49	0.19	3.1	10
710	5.4	1.4	0.74	59	4.85	3.02	79	70	215	0.41	4.8	20
1065	5.6	1.2	0.62	106	7.8	5.2	167	148	424	0.53	6.0	30
1775	6.6	1.0	0.42	209	13.3	9.26	389	343	919	0.69	7.9	50
3350	6.8	0.8	0.26	365	20	14.6	898	780	1964	0.73	10.8	100

TABLE IV. Calculated decay prior to equilibration for reactions of $^{16}O + {}^{60}Ni$ for $n=16$ (column headings are as defined in Table I).

E_{lab} ^{16}O (MeV)	$t_{eq} \times 10^{22}$ (sec)	$t_{fus} \times 10^{22}$ (sec)	$\frac{p_{11}}{p_{beam}}$	Δl ($\hbar$)	N_n	N_p	KE_n (MeV)	KE_p (MeV)	ΔE (MeV)	$\Delta E/E$	v_{rel}	$(E/A)_{c.m.}$ (MeV/nucleon)
202	5	1.8	0.92	7	0.61	0.69	6.5	10.7	28.6	0.18	3.1	10
405	5.0	1.4	0.76	24	2.21	2.35	38	51	129	0.40	4.1	20
606	5.6	0.8	0.62	62	3.84	3.96	85	105	259	0.54	6.9	30
1013	6.0	0.8	0.45	102	6.4	6.44	201	227	543	0.68	7.8	50
2027	6.4	0.6	0.27	190	10.1	9.9	489	514	1182	0.74	11.1	100

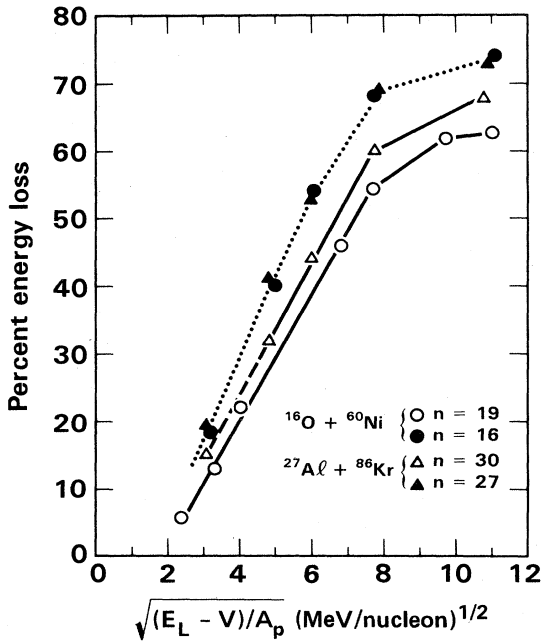

FIG. 3. Percent energy loss versus relative velocity for $^{16}O + {}^{60}Ni$ and $^{27}Al + {}^{86}Kr$ at c.m. energies of 10–100 MeV/nucleon. Calculated points from Tables I–IV are shown versus the relative velocity (abscissa) as defined in Table I. The calculated points have been joined by straight line segments as a visual guide. Calculated results are for initial exciton numbers equal to the projectile mass number (dotted curve) or three greater than the projectile mass number (solid and dashed curves).

therefore suggest an analysis in terms of a much cooler fissioning system, and of significantly lower mass, than given by the composite system mass and c.m. projectile energy. Precompound decay of nucleons should become of major importance as projectile energies go beyond 30 MeV/nucleon, and it is predicted to be a very significant process at somewhat lower energies.

B. Fractional linear momentum transfer and angular momentum decrement

1. Linear momentum transfer

The precompound nucleonic cascade described thus far should be related to the momentum transfer in heavy ion reactions. The factors necessary to completing the relationship which have not been addressed are the angular distribution of ejectiles and the contributions of non-nucleon ejectiles, e.g., α, d, t, etc. (A preliminary discussion of the linear momentum transfer question has already appeared.)

We will make some very simple assumptions and approximations for these points. For the angular distribution of nucleons, we begin by considering a diffraction limit to the angular distribution as first suggested by Mantzouranis *et al.*,[13]

$$R\Delta\theta \geq \hbar/k \tag{6}$$

where R is the nuclear radius, $\Delta\theta$ the angular uncertainty, and k the nucleon wave number. In Fig. 4 (from Ref. 14) we show the half-angle $\Delta\theta$ of Eq. (6) as a function of nucleon energy and nuclear mass number. In Figs. 5 and 6 (also from Ref. 14) we show the experimental angular distributions for neutrons of 9 and 14 MeV from the $^{90}Zr(p,n)$ reactions with 25 MeV (Refs. 15 and 16) incident protons, and for 20 and 30 MeV neutrons with 45 MeV incident protons.[16] The dotted curves in Figs. 5 and 6 represent the results of a calculation for which it was assumed that nucleons entering or leaving the nucleus are uniformly scattered (due to quantal processes) over a half-angle $\Delta\theta_{1/2}$ given by Eq. (6). For the case of a nucleon entering followed by a nucleon leaving the nucleus, we have folded the single scattering kernel with itself under the assumption that quantal phenomena such as refraction will be present in both entrance and exit channels. Greater detail and discussion of these results are to be found in Ref. 14. It may be seen that this result gives a quite good representation of the angular distributions over an angular range containing $\approx 80\%$ of the cross section.

The calculation used in generating the angular distribu-

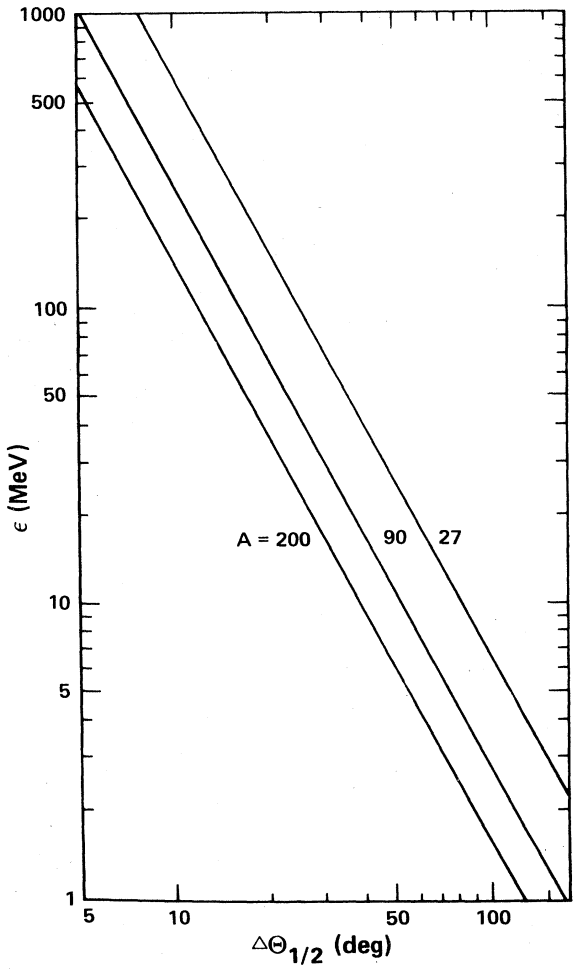

FIG. 4. The diffraction limit of angular constraint for nucleons versus nucleon energy for nuclei of mass number 27, 90, and 200. This figure is from Ref. 14 and results from Eq. (6).

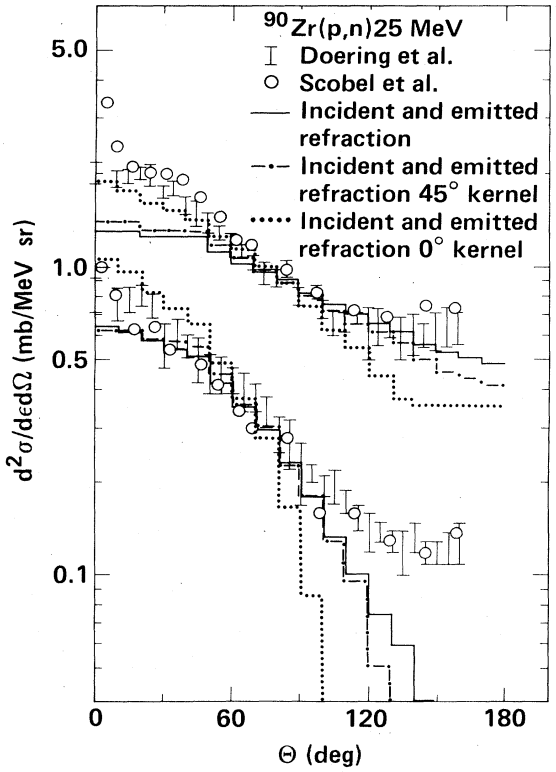

FIG. 5. Experimental and calculated neutron angular distributions for 25 MeV proton induced reactions on ^{90}Zr. Experimental results (circles and vertical bars, Refs. 15 and 16, respectively) are shown for 9 MeV (upper) and 14 MeV neutrons. The dotted angular distribution histogram results from folding the entrance channel and exit channel trajectories about the angles given by Eq. (6). This folding process is explained in detail in Ref. 14. The solid and dot-dash histograms represent a similar folding when an additional N-N scattering kernel is included.

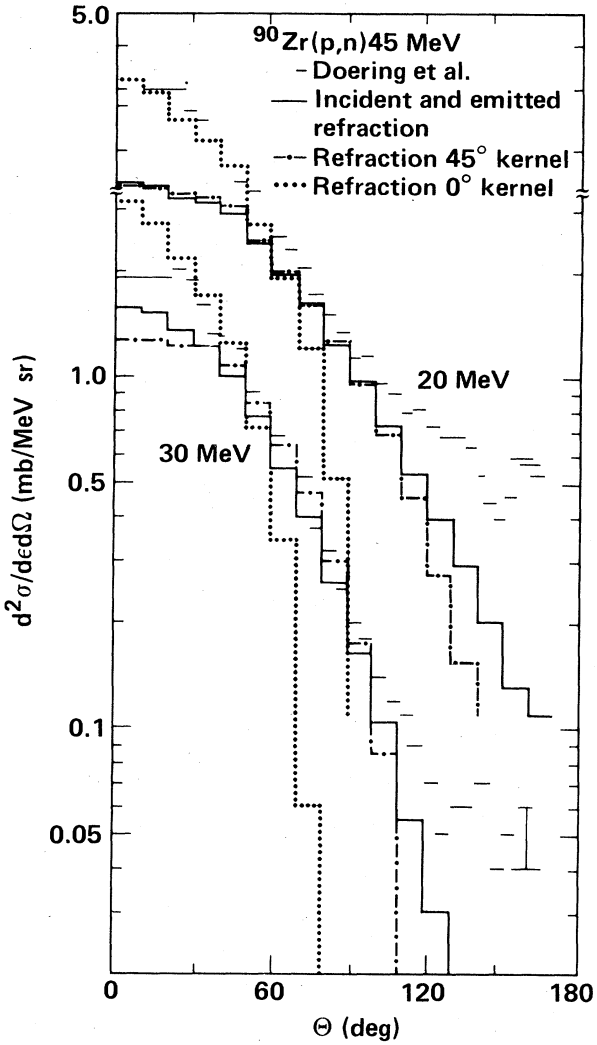

FIG. 6. As in Fig. 5 for 45 MeV incident protons and 20 and 30 MeV emitted neutron energies.

tions in Figs. 5 and 6 is too computationally tedious to use in the master equation approach, but does demonstrate that the diffraction angle limit is a reasonable one. Therefore we calculated the momentum decrement due to nucleon emission by multiplying the nucleon momentum by $\cos(\Delta\theta)$ from Eq. (6),

$$p_{11}=\sqrt{2M\epsilon}\cos(\Delta\theta) \tag{7}$$

if $\Delta\theta\leq 90°$, and by zero if $\Delta\theta>90°$. A value of $\Delta\theta>90°$ still will represent some forward peaking of the angular distribution. However, the forward peaking becomes slight when this is the case, so we make the isotropic assumption stated above for nucleons with a broad angular distribution. Figure 4 shows that these will be nucleons of a few MeV which should have undergone considerable relaxation toward equilibrium. In Eq. (7), M represents the nucleon mass and ϵ the kinetic energy.

The second point to consider is the influence of the emission of clusters such as d, t, α, etc., on the emission cascade. We have made a minimum correction to the momentum loss from the nucleon-cascade based on cluster multiplicities measured for reactions induced by 39, 62, and 90 MeV protons on a wide range of targets.[17,18] The ratios p:d:t:^{3}He:α were found roughly to be 10:1:0.02:0.02:0.5. We have used this ratio, assumed that it holds equally well for the neutron as well as proton cascade, and assumed a cluster kinetic energy of half the nucleon kinetic energy. This increases the momentum decrement by 8% over the pure nucleon cascade result. Because the correction under discussion is a small fraction of the total, a fairly large uncertainty in the assumed intensities and average energies would not seriously alter the results. Two points should be mentioned in this regard. The first is that in the inclusive measurements of Awes *et al.*[19] for ^{16}O + ^{197}Au, cluster multiplicities very much larger than those assumed in this work were observed. The second point is based on the model prediction of Bisplinghoff *et al.*[20] that high angular momenta should significantly enhance precompound cluster emission. In view of these considerations we must view our results as lower limits to the linear momentum loss, and observe that spectra of nucleons and clusters in coincidence with evaporation residues and fission fragments would be very valuable in constraining results of model precompound

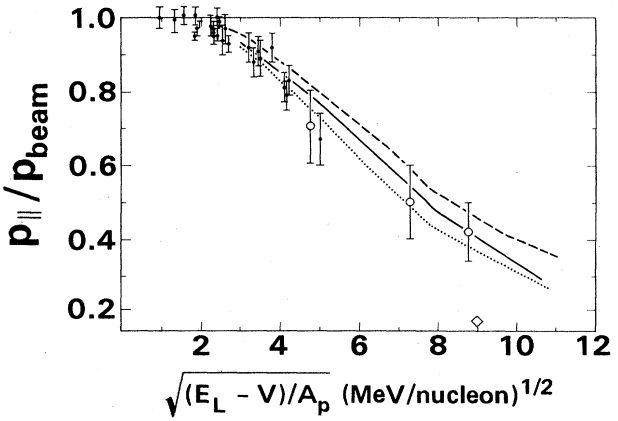

FIG. 7. Calculated and experimental linear momentum transfer for heavy ion reactions at energies up to 100 MeV/nucleon (c.m.). The ordinate gives the fraction linear momentum transfer; the abscissa is relative beam velocity as defined in Table I. The experimental result shown by closed circles with error bars are from the summary of Ref. 19; the original sources are to be found in Refs. 20–27. The open points with error bars are from Ref. 28, and the open triangle is from Ref. 29. The dashed curve is the calculated linear momentum transfer for ^{27}Al + ^{86}Kr assuming a 30 exciton energy partition; the solid curve is for ^{16}O + ^{60}Ni assuming a 19 exciton energy partition. The dotted curve is for ^{27}Al + ^{86}Kr assuming a 27 exciton partition, and for ^{16}O + ^{60}Ni assuming a 16 exciton partition.

decay calculations of linear momentum transfer in heavy ion reactions.

Results of the linear momentum calculation described are shown in Fig. 7 for the two test systems selected in this work. Various experimental results[21–31] are also shown in Fig. 7. Reference to Fig. 2(g) shows that the momentum transfer value has some sensitivity to the time assumed for equilibration. There is therefore some uncertainty in the calculated value due to subjectivity in selecting an equilibration time, and indeed all results quoted probably have a ±10% uncertainty for this reason alone. Nonetheless, the calculated results based on the sample phase space master equation model of Eqs. (1) and (2) are in very good agreement with the experimental results. We hope that this, coupled with the generally satisfactory reproduction of precompound nucleon spectra using exciton numbers in a reasonable range, suggests that the model reproduces the main aspects of the precompound-relaxation physics, although surely not the finer details. If this is so we might also estimate rough values of the angular momentum removed by the precompound cascade, as this could considerably alter the macroscopic trajectories of the interacting target-projectile systems. We consider this question in the following subsection.

2. *Angular momentum decrement in precompound cascade*

In the previous subsection we presented results based on the estimated forward component of momentum removed by the precompound decay cascade. This is semiclassically related to the angular momentum decrement by

$$l(\hbar)=p\times R=p_{11}\cdot R\ . \tag{8}$$

Where p is the momentum decrement and p_{11} and decrement parallel to the beam. To get some rough estimates of the angular momentum decrement we need only select a value of the radius. This could be done in any number of ways, but let us simply assume the composite system mass and a spherical system (recognizing that at very high angular momenta, equilibrium ground state shapes may have semimajor axes in excess of twice the spherical nucleus value). We will use an R_0 value of 1.5×10^{-13} cm, a "square well" value. Then if we let f be the calculated fractional linear momentum transfer from Tables I–IV, based on Eq. (7), ϵ_p the laboratory projectile energy, and A_p the projectile mass, the angular momentum removed by the precompound emission cascade may be estimated by

$$\begin{aligned}\Delta l(\hbar)&\simeq[(1-f)\sqrt{2A_p\epsilon_p}\,]R\\&\simeq0.34(1-f)\sqrt{A_p\epsilon_p}\,A_c^{1/3}\ .\end{aligned}\tag{9}$$

This is intended to give only a very rough estimate of the angular momentum removal possible due to the nucleon precompound decay. Results of using Eq. (9) for the two test systems are summarized in the fifth column of Tables I–IV. It may be seen that very significant angular momentum decrements may result from the precompound decay; many higher partial waves in the entrance channel may lead to compound nucleus formation than might have been expected by ignoring this phenomenon. Similarly higher partial waves and rotational energies will affect the initial exciton-energy partition in the coalescence process. We should not, therefore, be discouraged by the fact that a single initial exciton number does not reproduce the precompound spectra at all bombarding energies. We must first understand the dynamics of the reactions better before drawing quantitative conclusions about the model. Perhaps some better understanding of the ranges of the exciton parameter values versus bombarding energy would result from an iteration over distributions calculated using excitation energies decreased by rotational energies, using Eq. (9) with the output to get a range of relevant partial waves.

IV. CONCLUSIONS

We have used the Boltzmann master equation as a guide to the precompound nucleon emission cascade for reactions induced by heavy ions in the 10–100 MeV per nucleon region. The results will have a sensitivity to the initial exciton distribution assumed. As discussed, we do not understand all the macroscopic-microscopic details which would affect the exciton distribution, and the purpose of this work was not to investigate this potentially fertile area of physics. Rather we wished to see how the energy and precompound nucleon emission might vary with projectile energy. Because our simple excitation distribution function is reasonably successful in reproducing the experimental precompound spectra, our calculations should give guidance as to the expected precompound decay cascade versus projectile energy.

The results of the calculations are summarized in the

figures and in Tables I—IV. We see that very large fractions of the total energy are expected to be removed prior to equilibration at the higher energies considered, and that the residual composite system may have much lower angular momentum than is introduced in the entrance channel. This simple phase space calculation seems to give linear momentum transfer results which are quite consistent with experimental results.

Open questions include those of the multiplicities and spectral distributions of clusters emitted in coincidence with evaporation residue and fission fragments, and of the nucleon emission spectra for the same coincidence measurements. These data, extending beyond the 20 MeV/nucleon limit of Fig. 1, would allow better estimates of the reliability of the various calculated quantities summarized in Tables I—IV, and help decide if the result of Fig. 7 should be viewed as an upper limit only, or as a proper estimate of the fraction linear momentum transfer. In this way the crude calculation presented should become a more reliable tool for predicting the precompound decay contribution to energetic heavy ion reactions, and in developing a convenient time dependent model.

ACKNOWLEDGMENTS

The author is grateful to Dr. E. L. Pollock for providing the solution to the constrained exciton distribution problem, and the subroutine for evaluating Eqs. (4) and (5). This work was performed under the auspices of the U.S. Department of Energy by the Lawrence Livermore National Laboratory under Contract Number W-7405-ENG-48.

[1]G. D. Harp, J. M. Miller, and B. J. Berne, Phys. Rev. **165**, 1166 (1968).
[2]G. D. Harp and J. M. Miller, Phys. Rev. C **3**, 1847 (1971).
[3]M. Blann, A. Mignerey, and W. Scobel, Nukleonika **21**, 335 (1976).
[4]M. Blann, Phys. Rev. C **23**, 205 (1981).
[5]M. Blann, Annu. Rev. Nucl. Sci. **25**, 123 (1975).
[6]M. Blann, Nucl. Phys. **A235**, 211 (1974).
[7]J. Randrup, Ann. Phys. (N.Y.) **112**, 356 (1978).
[8]W. J. Swiatecki, Nucl. Phys. **A376**, 275 (1982).
[9]S. Cohen, F. Plasil, and W. J. Swiatecki, Ann. Phys. (N.Y.) **82**, 557 (1974).
[10]T. E. O. Ericson, Adv. Phys. **9**, 423 (1960).
[11]E. L. Pollock, private communication.
[12]E. Holub *et al.*, Phys. Rev. C **28**, 252 (1983).
[13]G. Mantzouranis, H. A. Weidenmuller, and D. Agassi, Z. Phys. A **276**, 145 (1976).
[14]M. Blann, W. Scobel, and E. Plechaty, Phys. Rev. C **30**, 1493 (1984).
[15]W. Scobel *et al.*, Phys. Rev. C **30**, 1480 (1984); Lawrence Livermore National Laboratory Report UCID-20101, 1984 (unpublished).
[16]M. Blann, R. R. Doering, A. Galonsky, D. M. Patterson, and F. E. Serr, Nucl. Phys. **A257**, 15 (1976).
[17]F. E. Bertrand, R. W. Peele, and C. Kalbach-Cline, Phys. Rev. C **10**, 1028 (1974).
[18]J. R. Wu, C. C. Chang, and H. D. Holmgren, Phys. Rev. C **19**, 698 (1979).
[19]T. C. Awes *et al.*, Phys. Rev. C **25**, 2361 (1982).
[20]J. Bisplinghoff and H. Keuser, in *Proceedings of the Workshop on Coincident Particle Emission From Continuum States in Nuclei, Bad Honnef, 1984, edited by H. Machner and P. Jahn (World Scientific,* Singapore, 1985), p. 195.
[21]Y. D. Chan *et al.*, Phys. Rev. C **27**, 447 (1983).
[22]B. B. Back *et al.*, Phys. Rev. C **22**, 1927 (1980).
[23]V. E. Viola *et al.*, Phys. Rev. C **26**, 178 (1982).
[24]H. Morgenstern *et al.*, Phys. Lett. **113B**, 463 (1982).
[25]E. Duek *et al.*, Z. Phys. A **307**, 221 (1982).
[26]W. J. Nicholson and I. Halpern, Phys. Rev. **116**, 175 (1958).
[27]S. S. Kapoor, H. Baba, and S. G. Thompson, Phys. Rev. **149**, 965 (1966).
[28]V. E. Viola *et al.*, Nucl. Phys. **A261**, 174 (1976).
[29]T. Sikkeland, E. L. Haines, and V. E. Viola, Jr., Phys. Rev. **125**, 1350 (1962).
[30]J. Galin *et al.*, Phys. Rev. Lett. **48**, 1787 (1982).
[31]J. Jastrebski, private communication.